*remote sensing*

MDPI

*Article*

# Neural Network Approach to Forecast Hourly Intense Rainfall Using GNSS Precipitable Water Vapor and Meteorological Sensors

**Pedro Benevides [1,*], Joao Catalao [2] and Giovanni Nico [3,4]**

1 Direção-Geral do Território (DGT), 1099-052 Lisbon, Portugal
2 Instituto Dom Luiz (IDL), Faculdade de Ciências, Universidade de Lisboa, 1749-016 Lisbon, Portugal; jcfernandes@fc.ul.pt
3 Istituto per le Applicazioni del Calcolo (IAC), Consiglio Nazionale delle Ricerche (CNR), 70126 Bari, Italy; g.nico@ba.iac.cnr.it
4 Department of Cartography and Geoinformatics, Institute of Earth Sciences, State University (SPSU), 199034 Saint Petersburg, Russia
* Correspondence: pbenevides@dgterritorio.pt

Received: 5 March 2019; Accepted: 18 April 2019; Published: 23 April 2019


**Abstract:** This work presents a methodology for the short-term forecast of intense rainfall based on a neural network and the integration of Global Navigation and Positioning System (GNSS) and meteorological data. Precipitable water vapor (PWV) derived from GNSS is combined with surface pressure, surface temperature and relative humidity obtained continuously from a ground-based meteorological station. Five years of GNSS data from one station in Lisbon, Portugal, are processed. Data for precipitation forecast are also collected from the meteorological station. Spaceborne Spinning Enhanced Visible and Infrared Imager (SEVIRI) data of cloud top measurements are also gathered, providing collocated information on an hourly basis. In previous studies it was found that the time-varying PWV is correlated with rainfall and can be used to detected heavy rain. However, a significant number of false positives were found, meaning that the evolution of PWV does not contain enough information to infer future rain. In this work, a nonlinear autoregressive exogenous neural network model (NARX) is used to process the GNSS and meteorological data to forecast the hourly precipitation. The proposed methodology improves the detection of intense rainfall events and reduces the number of false positives, with a good classification score varying from 63% up to 72% and a false positive rate of 36% down to 21%, for the tested years in the dataset. A score of 64% for intense rain events classification with 22% false positive rate is obtained for the most recent years. The method also achieves an almost 100% hit rate for the rain vs no rain detection, with close to no false alarms.

**Keywords:** global navigation satellite system (GNSS); precipitable water vapor (PWV); precipitation; meteorological sensors; spinning enhanced visible and infrared imager (SEVIRI); neural network; forecast

## 1. Introduction

Heavy rainfall phenomena are generally associated with moist convection processes characterized by a high variation in the water vapor content. The spatial and temporal rapid variations of the tropospheric water vapor in the low atmosphere poses one of the main challenges to the numerical weather models (NWMs) forecast accuracy [1]. Nowadays, the atmospheric measurement techniques are still insufficient to measure the tropospheric water vapor with the temporal and spatial resolution needed for the NWM precise forecasts [2]. The model's uncertainty regarding the water vapor

distribution limits its capability to identify instability situations, which can trigger heavy rain occurrences [3]. This particularity is even more crucial in the near real-time forecast (nowcast), since mechanisms of prevention and alarm are important to anticipate heavy rain episodes that can damage the population and its properties. Therefore, a better knowledge of the tropospheric water vapor state with the shortest possible latency is desirable in the meteorology community [4,5].

GNSS-derived tropospheric products are nowadays used in operational weather prediction applications and climate studies [5]. Some experiments based on GNSS atmospheric data have proved to be useful to study severe precipitation events [3,6,7]. A few assimilation experiments of GNSS tropospheric products into NWMs have proved to be beneficial to improve rainfall forecasts [1,8]. Furthermore, 3D water vapor maps derived from the GNSS tomography technique, using a regional network of stations, can provide additional information about the water vapor state [9]. The assimilation of water vapor information provided by GNSS techniques into an NWM can improve the model precision in severe storm situations, the same way it was verified with interferometric synthetic aperture radar (InSAR) data assimilation [2]. Regarding these applications, the near real-time GNSS processing strategies are important to be adopted, employing rapid orbits and clocks and precise point positioning processing [10].

In previous studies, it was found that the temporal variation of PWV measured by a GNSS sensor is correlated to rainfall, with a strong increase of PWV just before intense rainfall, followed by a decrease afterwards. However, a significant number of false positives were found, meaning that the evolution of PWV does not contain enough information to infer near future rain [11]. This study revealed that the probability of rain increases almost proportionally to statistical characteristics of PWV time series (PWV maximum, PWV variation and PWV rate of change), considering a time window of 6 hours after a PWV peak. This probability is close to 100% when these characteristics have higher values. However, at an hourly basis, a methodology based on the PWV rate of change forecasts 75% of the total rain and more than 90% of severe rain, with a false positive rate varying between 60% and 70%. Recently, other authors have developed similar techniques to forecast precipitation phenomena using GNSS data. Yao et al. [12] developed a similar short-term rainfall forecasting method tested in different regions of China, considering simultaneously the rate of change of PWV, the PWV variation and the monthly PWV. The results show a correct forecast of rainfall rate varying from 79% to 82%, with a 65% to 68% false alarm register. Manandhar et al. [13] proposed a simple method for rainfall nowcasting in tropical regions, using PWV absolute and second derivative values, also including seasonal-dependent values. Results from single stations in Singapore and Brazil revealed 85% to 87% true detection rate and a significant improvement of the false positive percentages, varying from 37% to 39%.

The GNSS-based forecast methods have generally demonstrated a high level of successful rainfall detection, which can be useful to assist NWM in the detection of heavy rainfalls. However, the significant number of false alarms hinder its actual application. In this work, we analyze the integration of PWV derived from GNSS with additional meteorological data into a neural network system, in order to improve the false positive rates of the short-term rainfall forecast. Very few studies using artificial neural networks with GNSS data applied to the meteorological field can be found in literature. The precipitation forecast using neural networks have been introduced in the 90s [14,15]. Some important studies have introduced the short-term forecast at a daily or hourly basis [16–19]. More recently, a study using a long short-term memory neural network method with 2D rainfall radar measurements to forecast up to 6 hours has improved the forecasts in rainy days due to the method's ability to monitor the spatial temporal sequence [20]. Other studies have used meteorological data and artificial intelligence techniques to forecast meteorological parameters related to GNSS, such as the total zenith delay [21], the weighted mean temperature [22] and also the PWV [23]. A nonlinear auto regressive approach with exogenous input (NARX) was used to perform real-time rainfall prediction combining daily rainfall from meteorological stations and GNSS PWV data [24]. This method is appropriated to learn long-term dependencies in a data time series. However, the results show correlations between

the input and predicted data lower than 0.50 for the test data, which may be due to the limited time series used in the study.

The aim of this work is to provide a new methodology to improve the performance of the rain forecast, relatively to the studies presented above, focusing on the intense rainfall short-term forecast. For this purpose, the integration of PWV data derived from GNSS and meteorological data is performed into a neural network system. The NARX technique is used to perform real-time rainfall prediction combining daily rainfall from a meteorological station. This neural network technique relies on long-term dependencies of a data time series being appropriate to study very dynamic systems based on the chaos theory, such as weather forecast. The network convergence is usually faster than regular neural network techniques, and the generalizations are also superior [25].

The integration of GNSS PWV data jointly with meteorological parameters into the neural network approach is expected to improve the detection of heavy rainfall events by reducing the large number of false positives obtained in the aforementioned studies. For this work, a continuous time series of 5 years of GNSS data in Lisbon, Portugal, are processed. Hourly measurements of PWV have been derived from GNSS processing. Continuous meteorological data such as surface pressure, surface temperature and relative humidity are obtained from ground-based meteorological stations. Remote sensing of cloud top data from Spinning Enhanced Visible and Infrared Image (SEVIRI) are also gathered. Five years of hourly accumulated precipitation data are also available for the neural network application.

## 2. Methods and Data Description

### *2.1. Neural Network Approach*

The neural network techniques are particularly well-suited to handle nonlinear problems, such as chaotic and rather unpredictable rainfall phenomena [15]. They can extract a general relationship between input and output data without prior physical and mathematical knowledge about the variables [21]. Its architecture is usually composed by one or a set of multilayers, with one or several neurons connected between them and running in parallel. The weight of each neuron is assigned and biased by a training function that evaluates the nonlinear relationships between the input and targets [16]. In this work we use a time series feedforward neural network model, the NARX model, to process a set of inputs in order to estimate a related set of target outputs, which in our case is the hourly precipitation. The NARX model can be represented by the following Equation (1),

$$y(t) = f\,(y(t-1), y(t-2), \ldots, y(t-n), x(t-1), x(t-2), \ldots, x(t-m)), \quad (1)$$

where $y(t)$ is the variable to be predicted, $x(t)$ the exogenous set of variables that relate to the variable of interest, $n$ the number of input delays of $y(t)$, $m$ the feedback delays of $x(t)$ and $f$ a nonlinear function. The model relates dynamically the time series of both current and past values of the variable to predict, at times $t$ and $(t-1)$, $(t-2)$, … , $(t-n)$, and the exogenous set of variables at times $(t-1)$, $(t-2)$, … , $(t-m)$, respectively. The variable $y(t)$ is predicted with the aid of its previous values, including external information $x(t)$ at its respective past values. A variant of this time series model is the particular case of the nonlinear autoregressive model without the exogenous inputs, usually defined as NAR (nonlinear autoregressive model), which is similar to Equation (1) but without the $x$ terms. The NAR is also a dynamic recurrent network just as the NARX network.

The neural network processing scheme can be divided into three distinct phases, each one of them with independent data sampling. The training phase evaluates the relationship between the variables input and the matching of the outputs, allowing to learn nonlinear relationships between them. The validation phase monitors the training performance, keeping the training going while generalized parameters have not been found. The test set is used to assess the network generalization performance. It is important to have a significantly large training sample in order to ensure that the model achieves viable results [21]. Despite the fact that prior knowledge between input-output

variables is not mandatory, the fitting of the results will be more adequate if consistency between the data is found [24].

### 2.2. Study Region

The Lisbon area, Portugal, was chosen as the study region. A 5-year time series of hourly registers related to meteorological parameters were collected from 2011 to 2015. A continuous series of PWV estimated from one GNSS station was processed. Pressure, temperature and relative humidity variables were also collected from a surface meteorological station. The GNSS and meteorological station are almost collocated, being only 1.25 km apart, as can be observed in Figure 1. In terms of altitude, the GNSS is located at 125 m height, whereas the meteorological station is 77 m above sea level, resulting in a vertical unevenness of less than 50 m. The meteorological station is named Geofísico and is managed by the Instituto Dom Luiz (IDL), being defined as an automatic principal station. The GNSS station is named IGP0 and belongs to the National Mapping Agency (DGT).

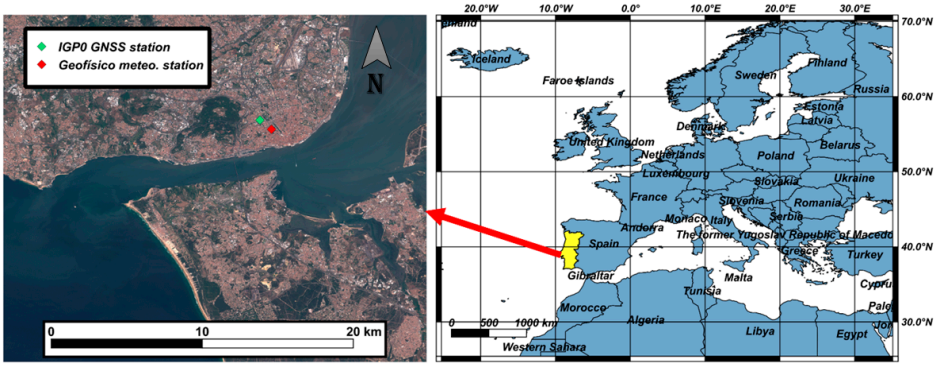


**Figure 1.** Location of the data used for this work within the Lisbon city area, Portugal, superimposed over a Sentinel-2 true color composition image.

### 2.3. SEVIRI Data

Remote sensing of cloud top data from SEVIRI were also gathered for the 5 year study period. SEVIRI is a multichannel spectrometer installed on board of the Meteosat Second Generation METEOSAT 9 satellite that can be used for different purposes, such as wind analysis, water vapor sensing and cloud tracking, and is capable of providing near real-time images. For this work, we focused on the cloud top proprieties of the atmosphere using the cloud top temperature (CTT), cloud top pressure (CTP) and cloud top height (CTH) variables. Cloud top properties data are produced by the Satellite Application Facility on Climate Monitoring (CM SAF) [26]. The CM SAF cloud property dataset level-2 products (CLAAS version 2) are produced continuously at a 15 min sampling rate with a large pixel size resolution of about 15 km. The region of interest used for this study is visualized in Figure 2. The final step was carried out, selecting the cloud top data pixel that contains in its interior the GNSS station.

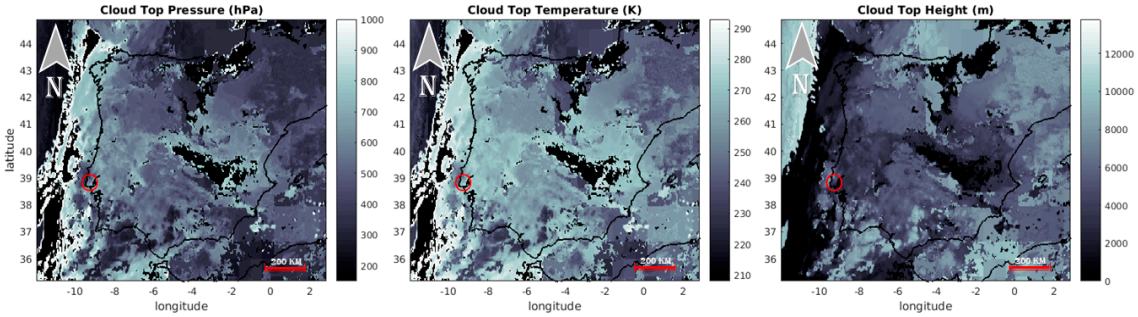


**Figure 2.** Cloud top temperature, pressure and height products representing the region of interest of the spaceborne Spinning Enhanced Visible and Infrared Imager (SEVIRI) images used for this study. The Lisbon area is marked with a red circle and the data corresponds to a heavy rain event that occurred on 26 October 2015 at 01:00 with a precipitation rate of 20 mm/h.

### *2.4. GNSS Data Processing*

The GNSS data processing was performed using the software package GAMIT (GNSS at MIT) and GLOBK (Global Kalman filter) [27]. The first one processes double-differenced phase data to estimate three-dimensional station coordinates, satellite orbits, Earth orientation parameters (EOP) as well as the atmospheric measurements in a loose a priori solution. The second uses a Kalman filter, combining the solution obtained from GAMIT with global geodetic solution experiments to accurately estimate a final parameter solution. Five years of RINEX data from IGP0 station were processed in daily double-difference sessions. Only GPS data were used in this study since the GAMIT/GLOBK version (v10.6) used in the processing did not include the multi-GNSS capability yet. Tight constraints to the ITRF14 (International Terrestrial Reference System 2014) were carried out. The ITRF14 used global station coordinates and EOP provided from GNSS and other space geodetic techniques data time series to update solutions from past years (i.e., 2008). A set of about 40 International GNSS Service (IGS) stations spread across the globe were grouped, in order to assure precise coordinate estimate and lower correlation for the atmospheric parameters. IGS precise final orbits were also used. The data processing was executed in two distinct steps to attain the best possible tropospheric results. The details of this methodology and its full parameterization can be found in Benevides et al. [28]. The zenith wet delay (ZWD) was the atmospheric parameter estimated for each station in the GNSS processing and was obtained at a time sampling of 15 min. The ZWD was related to the tropospheric water vapor, being converted to PWV using an empirical relationship calibrated to the regional climate of the study area [29,30].

### *2.5. Data Handling and Integration*

In order to create a consistent input configuration for the neural network processing, data derived from different sources (GNSS station, meteorological station and SEVIRI) had to be harmonized. Hence, the 15-min GNSS data sampling was averaged at a 1-hour rate to make it comparable with the hourly measurements available for the precipitation, pressure, temperature and relative humidity values provided by the meteorological station. The same procedure was executed for the cloud top variables obtained from SEVIRI, being each 15-min measurement averaged in each hour, therefore minimizing a larger portion of data with no registers. In this way, all the datasets were standardized and could be introduced together into the neural network.

## 3. Results and Discussion

### *3.1. Neural Network Configuration*

The primary variable used as the neural network input is the hourly precipitation. The group of external input variables is formed by the PWV obtained from the GNSS station, pressure, temperature

and relative humidity measured by the meteorological station and the CTT, CTP and CTH obtained from SEVIRI cloud products. A total of 41427 time steps are originated from the 5 years of continuous data. Table 1 summarizes the characteristics of the variables used in the neural network processing.

**Table 1.** Information regarding the neural network data variables used for this experiment.

| Variable Name | Source | Acronym | Units | Function |
|---|---|---|---|---|
| Hourly precipitation | Meteorological station | Rain | mm/h | Input/Output |
| Precipitable water vapor | GNSS station | PWV | mm | Input |
| Pressure | Meteorological station | P | hPa | Input |
| Temperature | Meteorological station | T | °C | Input |
| Relative Humidity | Meteorological station | RH | % | Input |
| Cloud Top Temperature | Remote sensing | CTT | K | Input |
| Cloud Top Pressure | Remote sensing | CTP | hPa | Input |
| Cloud Top Height | Remote sensing | CTH | m | Input |

The NARX network used for this work is initially configured with a set of default parameters. The network structure can be viewed in Figure 3. One hidden layer is selected for the input data with 10 neurons ($N$) and one output layer is selected for the targets with a single neuron ($M$). The number of feedback ($m$) and input delays ($n$) are set to be the number of hours associated with the weather nowcasting limit, which is 6 hours [20]. The network function used for the training step is the Levenberg–Marquardt algorithm, which is fast and does not require too much memory. The network's weight ($w$) and bias ($b$) structure is given by the architecture initially defined, relating the number of layers, neurons and inputs. The number of input weights is given by the number of neurons in the hidden layer (10) times the number of variables (8) and the number of input delays (6) resulting in a matrix with 480 elements. Additional parameters are the individual weight of each neuron and the respective bias for the input and output layers, resulting in 21 additional weight elements (10 + 10 + 1). The input and output variables are scaled before training between −1 and 1, so that the weights are comparable and not unit dependent.

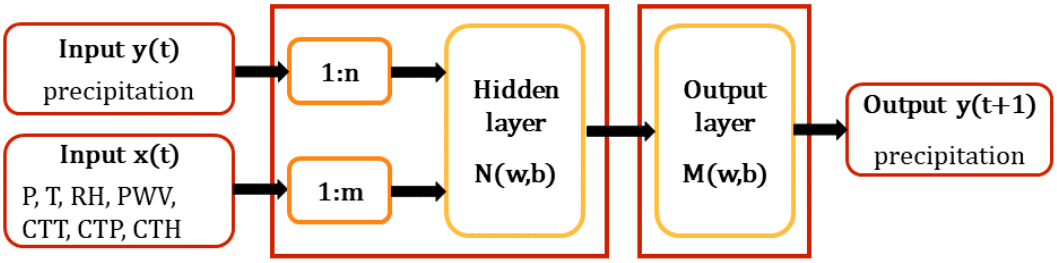


**Figure 3.** Structure of the nonlinear autoregressive exogenous neural network model (NARX) neural network model used in this work, where *y(t+1)* is the predicted variable, *y(t)* the input variable, *x(t)* the exogenous input variables, $n$ the input delays, $m$ the feedback delays, $N$ and $M$ the number of layer's neurons and $w$ and $b$ the respective weights and biases.

The data division is setup in order to process the neural network in two steps. The goal is to provide independent output precipitation values. In the first step we use a subset of 4 years of data (5 years in total), setting the larger portion to the training set, 66%, the shorter portion to the validation set, 10%, and 24% of the portion to the test. This way we assure that about 1 year of data is used for results assessment. The sample selection for the data division is done randomly. In the second processing step the trained network from the first step is used to forecast the rain using 1 year of data not used in the training. Since the training is performed with a different data subset (4 years), the output predicted precipitation values for one year are obtained in an independent manner. Table 2 summarizes the most important parameters of the neural network. The hourly precipitation continuous data is characterized by its rapid temporal variability, including most cases of no rain to moderated rain

episodes and the more complex intense rainfall patterns, which are statistically not frequent. For this reason, we have chosen to sum the rain values forward in time, but not surpassing the nowcasting window threshold of 6 hours. This sum time window has been set initially and just for the precipitation values, as 1 hour forward. A set of 100 runs is defined for each experiment, since the initial weights are randomly generated in the neural network training phase, therefore affecting the fitting output results. Consequently, the results are assessed in each experiment considering the mean or maximum values obtained from the total number of runs.

**Table 2.** Information regarding the neural network default or initial parameters used for this work.

| Variable Name | Values |
|---|---|
| # Hidden layers | 1 |
| # Neurons | 10 |
| # Delays | 6 |
| Training function | Levenberg-Marquardt |
| Data weighting | Random |
| Performance evaluation | Mean square error |
| Data division | Step 1: (66%/10%/24%)—4 years |
| (training/validation/testing) | Step 2: (0%/0%/100%)—1 year |
| # Total input variables | 8 |
| # Output variables | 1 |
| # Number of samples | 41427 |

In order to better assess the potentiality of the method to forecast heavy precipitation, a classification of the precipitation intensity is implemented. Thus, three classes are defined for the target and output hourly precipitation, which are a class for non-raining values, an intermediated class regarding moderated rain with values higher than 0 and lower than 5 mm/h and a final class corresponding to more intense rain containing all values with precipitation reaching at least 5 mm/h. This threshold is chosen considering the rain intensities observed in the region of study, where it is found that these events at a rate of one hour represent about 0.5% of the total of rain occurrences during the study period. Thereby, it can be stated that the intense rain in this region is considered as a rare event. The precipitation classes and the number of trends can be observed in Table 3. This classification is applied to the target rain values, considered as the measured or reference values and also applied to the output data resulting from the neural network output. The classification for the output data considers a 0.5 mm/h tolerance in the moderated and intense rain classes. With this simple class clustering we can test more clearly the capability of this method to identify correctly the heavy rain events.

**Table 3.** Details of the classification of precipitation data and the corresponding number of observations concerning the neural network data division.

| Precipitation Class | Rain Classification (mm/h) | Number of Samples (hour) | | |
|---|---|---|---|---|
| | | 4 Years | 1 Year | Total |
| No rain | 0 | 31284 | 7527 | 38811 |
| Moderated rain | $> 0 < 5$ | 2184 | 252 | 2436 |
| Intense rain | $>= 5$ | 159 | 22 | 181 |

### 3.2. Network Sensitivity to Parameters

The first experiment was performed varying some of the initial parameters described in Table 2, such as the number of default feedback and input delays, the number of hidden neurons and the training function. The goal was to verify the possibility to improve the results obtained with the default parameters. Nevertheless, some configurations were maintained, such as the number of input variables and data division. The 4 years used in the data division of step 1 are 2011 to 2014, and for step 2 the remaining year 2015 was used for the assessment of results. The mean value was computed over

100 runs, for all the experiments. A statistical summary of the results is presented in Table 4, focusing on the good classification and false positive percentages of the intense rain class. The percentage of correctly classified intense rain was evaluated, relating the number of well-classified intense rain events by the neural network processing with the real or observed rain values (in Table 3). The false positive percentage was calculated, evaluating the total number of intense rain events wrongly classified by the neural network experiment as intense rain. The statistical assessments also included the network prediction error (Net.RMS), which is a mean squared normalized error calculated between the output network values and the observed precipitation values, and the correlation coefficient for the step 2 dataset. The reference result values were obtained when using the network defaults parameters, leading to a good classification percentage of 59.1%, with a 29.6% percentage of false positives, a network RMS of 0.467 and a network correlation coefficient of about 0.824. The major differences between the experiments summarized in Table 4 were obtained for the false positive percentages of the intense rain.

**Table 4.** Statistical assessment of the neural network experiments, comparing the initial and optimized network parameters. Results correspond to the mean value score for 100 runs. Good classification and false positives are presented in % of intense rain class, and network RMS is in mm/h.

| Neural Network with 7 Variables (GNSS+Meteo+Sat.) | Intense Rain Class | | Test Dataset | |
|---|---|---|---|---|
| | Good Classification | False Positives | Net.RMS | Correlation Coefficient |
| 10 N, 6 ID 6 FD, Levenberg-Marquardt | 59.1% | 29.6% | 0.467 | 0.824 |
| 10 N, **8 ID 8 FD**, Levenberg-Marquardt | 59.1% | 28.7% | 0.470 | 0.821 |
| **2 N**, 6 ID 6 FD, Levenberg-Marquardt | 59.1% | 26.4% | 0.472 | 0.818 |
| 10 N, 6 ID 6 FD, **Bayesian regularization** | 59.1% | 26.0% | 0.489 | 0.803 |

The first tested parameter was the number of default feedback (FD) and input delay (ID) values. These parameters varied equally between 1 to 10 delays. Similar intense classification results were obtained with 1 to 4 delays, showing, however, larger false positive rate, higher network error and smaller correlation. When testing with a number of 8 delays, the results were very similar to the default ones (6 delays), showing similar good classification, error and correlation, while presenting a small improvement on the false positive rate (28.7%). Increasing the number of delays to 10 resulted in the same levels of error and correlation but it significantly increased the false positives rate. The configuration of unbalanced delays was also tested with combinations of input delays and feedback delays varying from 1 to 6. However, none of these configurations have provided better results for the intense rain classification.

The following tested parameter was the neural network number of neurons. Experiments were performed varying the neurons in the hidden layer from 1 to 25. Overall, the number of good classifications remained unchanged, but the number of false positives decreased with fewer neurons in the network. When using 1 neuron, the number of false positives was the lowest (22.2%), but with a significant diminishment in the good classification of intense rain, higher network RMS and lower correlation. However, when using 2 neurons the network reached 59.1% for good classification and 26.4% for false positive percentage, outperforming the intense rain classification for the default values. Increasing the neurons by more than 2 did not improve the percentage of good classification, and moreover it increased the false positive percentage. Additional tests extending the network complexity with extra hidden layers were performed (see Figure 3). However, it was verified that as the number of hidden layers increased, the percentage of good classification and correlation decreased, and the false positive rate increased as well as the network error.

The final parameter testing was performed with the network training function. The neural network initial parameters were restored again (10 neurons with 6 delays). We have chosen the training functions that are most commonly used in this technique [31]. The statistical assessment using the

Quasi-Newton and Conjugate gradient training functions (not shown) revealed very poor results when compared to the default Levenberg-Marquardt function. However, the Bayesian regularization function achieved the same good classification percentage and managed to drop the false positive percentage by more than 3% (26%) without a significant increase in the network error and a slight decrease in the global correlation coefficient. The parameter variation experiments over the neural network initial values and its statistical analysis of the intense rain classification revealed that some parameters can be modified from the default values in order to improve the results. In the following sections, the best individual parameters identified in these experiments—the 2 neurons with one hidden layer, 8 delays and Bayesian regularization training function—are combined for additional neural network proprieties testing.

### 3.3. Network Sensitivity to Input Variables

A set of tests was performed varying the number of input variables to better understand the sensitivity of the neural network in terms of intense rain classification. In particular, given the indicators of previous studies, emphasis was placed on the GNSS PWV. The network configuration from Table 2 was used together with the implementation of the optimized network parameters determined from the previous section (Table 4). The test results are presented in Table 5. The input configuration with 7 variables and optimized parameters achieved an improvement of about 3% in the false positive percentage, maintaining the same percentage of good classification compared with the initial configuration result. When combining the GNSS and meteorological station variables, the percentage of good classification slightly increased, and the false positive percentage also increased to the maximum value of the experiment (27%). Processing the neural network with the PWV as the only input resulted in a marginal higher good classification percentage (59.3%) and the lowest percentage of false positives (22.6%). The last experiment was performed with a slight variation of the NARX model configuration, which was running the network in NAR configuration mode, i.e., using only the *y(t)* precipitation as input (see Figure 3). The NAR results show the smallest percentage of good classification (58.2%) with a similar false positives percentage to that obtained for the PWV input configuration.

**Table 5.** Statistical assessment of the neural network input experiments with 4 different input configurations, using optimized parameters. Results correspond to the mean value score for 100 runs. Good classification and false positives are presented in % of intense rain class and Network RMS is in mm/h.

| Neural Network with 7 Variables (GNSS+Meteo+Satellite) | # var. | Intense Rain Class | | Test Dataset | |
|---|---|---|---|---|---|
| | | Good Classification | False Positives | Net.RMS | Correlation Coefficient |
| GNSS + Meteo. + Satellite (PWV,P,T,RH,CTT,CTP,CTH) | 7 | 59.1% | 26.5% | 0.475 | 0.819 |
| GNSS + Meteo. (PWV,P,T,RH) | 4 | 58.9% | 27.1% | 0.471 | 0.821 |
| GNSS (PWV) | 1 | 59.3% | 22.6% | 0.471 | 0.817 |
| Precipitation (NAR model) | 1 | 58.2% | 22.7% | 0.474 | 0.815 |

The network error and correlation coefficient of the optimized experiments are marginally larger than that observed for the initial network configuration. This is probably related to the decrease in the number of neurons, as it was verified in the previous section. However, between these experiments, the error and correlation variations are very small, the best score being obtained for the 4 exogenous input variables. Summarizing the results of this experiment, it was observed that introducing more variables into the neural network processing does not produce the better results. The best classification scores of the intense rain events are obtained for the input exogenous configuration with GNSS PWV. When introducing more external variables from different sources (meteorological station and satellite SEVIRI cloud top data) the network error generally increases.

### *3.4. Network Sensitivity to Data Division*

In this section, the neural network sensitivity is evaluated, varying the data division in time. The data division configuration defined in the neural network configuration section is modified, setting up experiments using each year of the full 5-year dataset as a test year (step 2 of Table 2). The remaining data in each experiment are evenly distributed by the training, validation and test of step 1, keeping the percentages of data division previously defined in Table 2. These experiments consider the neural network optimized configuration. A helpful indicator for the nowcasting of heavy rain is to consider the maximum value from the 100 runs processed in each experiment, which is derived from the highest percentage of good classification and lowest percentage of false positives of the intense rain class. The input configuration used for this experiment is the exogenous input PWV variable.

The statistical assessment shown in Table 6 shows quite stable performances in the intense rain classification. These results seem also to confirm that we are not faced with the overfitting problem. The 2013 dataset has the lowest percentage of false positives (21%) with a high percentage of good classification (66%), also showing intermediate intense rain events (37). The year with the poorer intense rain classification is 2011, with the smallest good classification (63%) and the highest percentage of false positives (36%), although being characterized by the highest number of intense rain events (57). The 2015 dataset has similar good classification score but with a much lower false positive rate (22%), being also the year with the smallest number of intense rain events (22), an indicator of a dryer year. The year 2012 shows the highest percentage of good classification, reaching 72% with a relatively low false positive percentage of 23%, showing a relatively small network error (0.59) and the highest correlation coefficient (0.88). The higher variability in the neural network performance in this test is a direct consequence of a different number of intense rain data registered in each year. However, the variability in the network error and correlation also suggests that the data available for the training and validation steps may not be sufficient to provide a robust model for the intense rain prediction in all weather conditions. On the other hand, the smaller network error obtained in the 2015 dataset is a consequence of the testing period being all continuous, that is, not being interrupted by a segmented year from the middle of the dataset. Nevertheless, the result of this experiment shows that the methodology presented here has potential to be used as a tool for assisting in the intense rain forecast nowcasting. Comparing with results from previous studies introduced in Section 1 [11–13], and even though these studies consider all the types of rain, a significant improvement in the false positive rate with registers of 36% down to 21% is observed, just considering the heavy rain events. The following section explores in more detail the properties of the neural network for the dataset in continuous mode, using the most recent year (2015) for results assessment.

**Table 6.** Statistical assessment of the neural network experiment with variations in the data division. Optimized parameters and PWV exogenous input variable configuration is considered. Results correspond to the maximum value score for 100 runs. Good classification and false positives are presented in % of intense rain class, and Network RMS is in mm/h.

| Neural Network with 7 Variables (GNSS+Meteo+Satellite) | #Intense Rain | Intense Rain Class | | Test Dataset | |
|---|---|---|---|---|---|
| | | Good Classification | False Positives | Net.RMS | Correlation Coefficient |
| 2015 test dataset | 22 | 63.6% | 22.2% | 0.464 | 0.826 |
| 2011 test dataset | 57 | 63.3% | 35.6% | 0.875 | 0.828 |
| 2012 test dataset | 32 | 71.9% | 23.3% | 0.589 | 0.875 |
| 2013 test dataset | 37 | 66.0% | 20.5% | 0.807 | 0.820 |
| 2014 test dataset | 41 | 64.3% | 30.8% | 0.726 | 0.831 |

### *3.5. Best Case with Optimized Parameters*

The best result for the most recent year of the data series is analyzed here (optimized parameters 2 neurons with one hidden layer, 8 delays and Bayesian regularization training function, GNSS PWV, one

exogenous variable configuration, best intense rain score in 100 runs for the 2015 test dataset). Figure 4 shows hourly the rainfall in situ measurements and forecasts provided by the neural network output. These values are concentrated in the region of low-intensity rainfalls, smaller than 5 mm/h, and have a correlation coefficient of 0.83. The differences between the predicted and observed values increase gradually, not predicting some of the higher observed rain events. The comparison of predicted and observed values through the year 2015 shows a good coverage of the rain events, where the predicted values seem to be more underestimated than overestimated. Different rainfall patterns can be observed throughout the year, with a drier period from July to September, and some rainier months like January, April and October. Most of the output values are concentrated in the region around zero, with a more noticeable noisy concentration of rainfall values in the month of October.

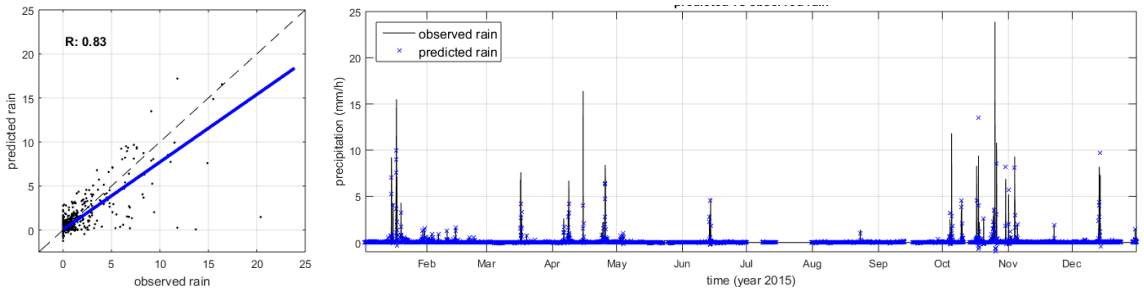


(**a**) (**b**)

**Figure 4.** Linear fitting between the predicted rain values from the neural network and the observed rain values, in units of mm/h, for the year 2015 (**a**). The same comparison is illustrated for all values of the year 2015 organized by time (**b**). Results correspond to the best score for 100 runs with the initial network parameters set in Table 2.

As a further assessment of the proposed methodology, a confusion matrix is used to assess the classification results of the whole rainfall datasets. Figure 5 summarizes the results of the confusion matrix. In this form we can evaluate the precipitation considering the classification of the output values (row-wise) versus the classification of the reference or measured values (column wise), also known as the ground truth. The matrix shows all the 2015 dataset precipitation values distributed by classes, where the diagonal position represents the number of correctly classified precipitation events. The marginal bottom row shows the global percentage of correctly classified trends obtained for the output values (green percentage) with respect to the measured values, and also the percentage of omission errors for each class (red percentage), determined from the non-diagonal overclassified events. As for the marginal right end column, it identifies for the classification output, the percentage of correctly classified events in each class (green percentage) and its commission error or false positive rate (red percentage). The highest ground truth classification is obtained for the no rain class, with almost 100% of well-classified events, followed by the intense rain with about 64% and the moderated rain with 35%. As for the output classification, the no rain also has the highest score, with 98%. The moderated rain also has a better classification score with 77% of the values well-classified, while the class of interest, the intense rain, manages to achieve about 78% well-classified output events with a false positive rate of about 22%. The overall classification accuracy is very good, achieving 97.5%. In addition to the previously demonstrated neural network capacity to forecast heavy rain events with high correctness and low false positive rate, the confusion matrix shows that this method has also a remarkable hit success for the no rain events, being near 100%. This property can be useful in meteorological applications where the knowledge of the rain/no rain factor is important, such as precision farming.

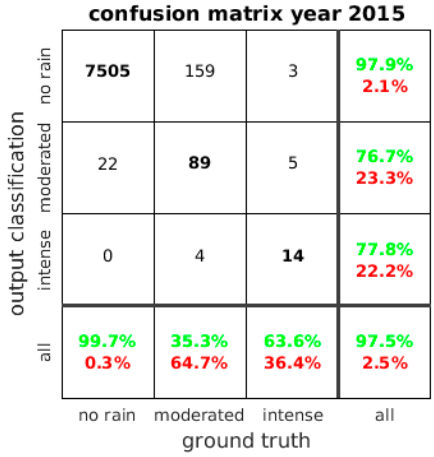


**Figure 5.** Confusion matrix relating the precipitation forecast provided by the neural network output and the observed or measured rainfall input (ground truth), classified after the neural network result using Table 3. Results correspond to the best score for 100 runs with the optimized network parameters (2 neurons, 1 hidden layer, 8 feedback and input delays and Bayesian training), Global Navigation Satellite System (GNSS) precipitable water vapor (PWV) one input variable configuration and test dataset 2015.

## 4. Conclusions

A large dataset of continuous GNSS measurements of PWV, meteorological measurements and spaceborne SEVIRI images has been analyzed by means of neural network NARX method. The goal was to find a relationship between atmospheric and cloud properties and in situ rainfall measurements to be used for the nowcasting of intense rain events. A total set of 7 variables obtained from GNSS and meteorological measurements were gathered, corresponding to five years of continuous data, and introduced into the neural network in order to estimate hourly precipitation. Classification of output results is performed in three rain classes to assess the method's intense rain forecast skill. Several experiments have been carried out with different initial conditions for the neural network parameters. For each parameter's configuration, a set of 100 runs was used for the statistical assessment of forecast results. Tests evaluating the neural network sensitivity to different parameters found that the best results for the classification of intense rain events were obtained for network configuration of 2 neurons, 1 hidden layer, 8 feedback and input delays and Bayesian regularization training. Tests performed varying the number of the neural network exogenous variables revealed that using all input variables, including data from meteorological station and cloud top information from SEVIRI images, resulted in a reduced capability of the neural network to correctly classify the intense rain events. Better classification results were obtained when using only the GNSS PWV variable (64% good classification, 22% false positives). The reason for this could be related to the different acquisition proprieties regarding the ground-based GNSS and meteorological stations, and the spaceborne SEVIRI imaging. GNSS uses a mean of all satellite observations to estimate the total column of PWV, which is basically referring to the lower tropospheric layer, while the metrological station measures quantities at the surface level. On the other hand, SEVIRI is measuring the quantities at the top of the clouds (see Figure 2 for the statistical distribution of cloud heights), not observing most of the time, the same portion of troposphere as the ground sensors, particularly in the presence of clouds, which are the rain trigger. Therefore, the physical quantities of the GNSS, metrological station and SEVIRI are poorly correlated, and the lower part of the troposphere sensed from the GNSS stations could be more important to study the precipitation behavior.

Comparisons with previous studies showed that the proposed methodology has a better performance, achieving a significant reduction in the severe rain false positives forecast. The experiment evaluating the network sensitivity to different years of independent measurements revealed very distinct results, probably due to the number of intense rain events registered in each year. Longer time

series of many years would be desirable, as well as other GNSS location, in order to better model the complex behavior of the precipitation phenomena and its different regimes observed even in consecutive years. These results support the idea of the usefulness of a data-driven analysis of atmospheric and rainfall measurements based on a neural network methodology in applied meteorology as an auxiliary tool for the short-term forecast of heavy rainfall events. As a co-product of this study, it has been observed that the presented methodology has a near 100% hit success for the no rain event classification, with almost no false positives. This result can be of interest in applications tightly related to applied meteorology, such as precision farming, where the information of a lack of rainfalls has an important economic value in agricultural practices.

**Author Contributions:** Conceptualization, J.C. and P.B.; methodology, J.C. and P.B.; validation, P.B.; formal analysis, P.B.; investigation, P.B., J.C. and G.N.; writing—original draft preparation, P.B.; writing—review and editing, P.B., J.C. and G.N.; visualization, P.B.; supervision, J.C. and G.N.

**Funding:** This research was funded by Fundação para a Ciência e Tecnologia (FCT), project UID/GEO/50019/2019—Instituto Dom Luiz.

**Acknowledgments:** The authors would like to thank the DGT for providing freely the GNSS data and the CM SAF for providing freely the SEVIRI cloud property dataset level-2 products.

**Conflicts of Interest:** The authors declare no conflict of interest.

## References

1. Yan, X.; Ducrocq, V.; Poli, P.; Hakam, M.; Jaubert, G.; Walpersdorf, A. Impact of GPS zenith delay assimilation on convective-scale prediction of Mediterranean heavy rainfall. *J. Geophys. Res. Atmos.* **2009**, *114*. [CrossRef]
2. Mateus, P.; Miranda, P.M.A.; Nico, G.; Catalão, J.; Pinto, P.; Tomé, R. Assimilating InSAR maps of water vapor to improve heavy rainfall forecasts: A case study with two successive storms. *J. Geophys. Res. Atmos.* **2018**, *123*, 3341–3355. [CrossRef]
3. Brenot, H.; Neméghaire, J.; Delobbe, L.; Clerbaux, N.; De Meutter, P.; Deckmyn, A.; Delcloo, A.; Frappez, L.; Van Roozendael, M. Preliminary signs of the initiation of deep convection by GNSS. *Atmos. Chem. Phys.* **2013**, *13*, 5425–5449. [CrossRef]
4. Mateus, P.; Nico, G.; Catalao, J. Uncertainty Assessment of the Estimated Atmospheric Delay Obtained by a Numerical Weather Model (NMW). *IEEE Trans. Geosci. Remote Sens.* **2015**, *53*, 6710–6717. [CrossRef]
5. Guerova, G.; Jones, J.; Douša, J.; Dick, G.; Haan, S.D.; Pottiaux, E.; Bock, O.; Pacione, R.; Elgered, G.; Vedel, H.; et al. Review of the state of the art and future prospects of the ground-based GNSS meteorology in Europe. *Atmos. Meas. Tech.* **2016**, *9*, 5385–5406. [CrossRef]
6. Suparta, W.; Ali, M. Nowcasting the lightning activity in Peninsular Malaysia using the GPS PWV during the 2009 intermonsoons. *Ann. Geophys.* **2014**, *57*, A0217. [CrossRef]
7. Barindelli, S.; Realini, E.; Venuti, G.; Fermi, A.; Gatti, A. Detection of water vapor time variations associated with heavy rain in northern Italy by geodetic and low-cost GNSS receivers. *Earth Planets Space* **2018**, *70*, 28. [CrossRef]
8. De Haan, S. Assimilation of GNSS ZTD and radar radial velocity for the benefit of very-short-range regional weather forecasts. *Q. J. R. Meteorol. Soc.* **2013**, *139*, 2097–2107. [CrossRef]
9. Benevides, P.; Nico, G.; Catalao, J.; Miranda, P.M.A. Analysis of Galileo and GPS Integration for GNSS Tomography. *IEEE Trans. Geosci. Remote Sens.* **2017**, *55*, 1936–1943. [CrossRef]
10. Dousa, J.; Vaclavovic, P. Real-time zenith tropospheric delays in support of numerical weather prediction applications. *Adv. Space Res.* **2014**, *53*, 1347–1358. [CrossRef]
11. Benevides, P.; Catalao, J.; Miranda, P.M.A. On the inclusion of GPS precipitable water vapour in the nowcasting of rainfall. *Nat. Hazards Earth Syst. Sci.* **2015**, *15*, 2605–2616. [CrossRef]
12. Yao, Y.; Shan, L.; Zhao, Q. Establishing a method of short-term rainfall forecasting based on GNSS-derived PWV and its application. *Sci. Rep.* **2017**, *7*, 12465. [CrossRef]
13. Manandhar, S.; Lee, Y.H.; Meng, Y.S.; Yuan, F.; Ong, J.T. GPS-Derived PWV for Rainfall Nowcasting in Tropical Region. *IEEE Trans. Geosci. Remote Sens.* **2018**, *56*, 4835–4844. [CrossRef]
14. French, M.N.; Krajewski, W.F.; Cuykendall, R.R. Rainfall forecasting in space and time using a neural network. *J. Hydrol.* **1992**, *137*, 1–31. [CrossRef]

15. Hall, T.; Brooks, H.E.; Doswell III, C.A. Precipitation forecasting using a neural network. *Weather Forecast.* **1999**, *14*, 338–345. [CrossRef]
16. Ramirez, M.C.V.; de Campos Velho, H.F.; Ferreira, N.J. Artificial neural network technique for rainfall forecasting applied to the Sao Paulo region. *J. Hydrol.* **2005**, *301*, 146–162. [CrossRef]
17. Rivolta, G.; Marzano, F.S.; Coppola, E.; Verdecchia, M. Artificial neural-network technique for precipitation nowcasting from satellite imagery. *Adv. Geosci.* **2006**, *7*, 97–103. [CrossRef]
18. Hung, N.Q.; Babel, M.S.; Weesakul, S.; Tripathi, N.K. An artificial neural network model for rainfall forecasting in Bangkok, Thailand. *Hydrol. Earth Syst. Sci.* **2009**, *13*, 1413–1425. [CrossRef]
19. Wu, C.L.; Chau, K.W.; Fan, C. Prediction of rainfall time series using modular artificial neural networks coupled with data-preprocessing techniques. *J. Hydrol.* **2010**, *389*, 146–167. [CrossRef]
20. Shi, X.; Chen, Z.; Wang, H.; Yeung, D.Y.; Wong, W.K.; Woo, W.C. Convolutional LSTM network: A machine learning approach for precipitation nowcasting. In Proceedings of the Advances in Neural Information Processing Systems, Montreal, QC, Canada, 7–12 December 2015; pp. 802–810.
21. Suparta, W.; Alhasa, K.M. Modeling of zenith path delay over Antarctica using an adaptive neuro fuzzy inference system technique. *Expert Syst. Appl.* **2015**, *42*, 1050–1064. [CrossRef]
22. Ding, M. A neural network model for predicting weighted mean temperature. *J. Geod.* **2018**, *92*, 1187–1198. [CrossRef]
23. Suparta, W.; Alhasa, K.M. Modeling of precipitable water vapor using an adaptive neuro-fuzzy inference system in the absence of the GPS network. *J. Appl. Meteorol. Climatol.* **2016**, *55*, 2283–2300. [CrossRef]
24. Rahimi, Z.; Shafri, H.Z.M.; Norman, M. A GNSS-based weather forecasting approach using Nonlinear Auto Regressive Approach with Exogenous Input (NARX). *J. Atmos. Sol.-Terr. Phys.* **2018**, *178*, 74–84. [CrossRef]
25. Lin, T.; Horne, B.G.; Tino, P.; Giles, C.L. Learning long-term dependencies in NARX recurrent neural networks. *IEEE Trans. Neural Netw.* **1996**, *7*, 1329–1338. [CrossRef]
26. Finkensieper, S.; Meirink, J.F.; van Zadelhoff, G.J.; Hanschmann, T.; Benas, N.; Stengel, M.; Fuchs, P.; Hollmann, R.; Werscheck, M. CLAAS-2: CM SAF CLoud Property dAtAset Using SEVIRI. Available online: https://bit.ly/2GrdHU2 (accessed on 22 April 2019).
27. Herring, T.; King, R.W.; McClusky, S.C. *GAMIT Reference Manual—GPS Analysis at MIT—Release 10.4*; Department of Earth, Atmospheric and Planetary Sciences, MIT: Cambridge, MA, USA, 2010.
28. Benevides, P.; Catalao, J.; Nico, G.; Miranda, P.M.A. 4D wet refractivity estimation in the atmosphere using GNSS tomography initialized by radiosonde and AIRS measurements: Results from a 1-week intensive campaign. *GPS Solut.* **2018**, *22*, 91. [CrossRef]
29. Bevis, M.; Businger, S.; Herring, T.; Rocken, C.; Anthes, R.A.; Ware, R.H. GPS meteorology: Remote sensing of the atmospheric water vapor using the Global Positioning System. *J. Geophys. Res.* **1992**, *97*, 15787–15801. [CrossRef]
30. Mateus, P.; Nico, G.; Catalão, J. Maps of PWV temporal changes by SAR interferometry: A study on the properties of atmosphere's temperature profiles. *IEEE Geosci. Remote Sens. Lett.* **2014**, *11*, 2065–2069. [CrossRef]
31. Yaghini, M.; Khoshraftar, M.M.; Fallahi, M. A hybrid algorithm for artificial neural network training. *Eng. Appl. Artif. Intell.* **2013**, *26*, 293–301. [CrossRef]